Photocatalytic removal of nitric oxide by $Bi_2Mo_3O_{12}$ prepared by co-precipitation method

E. Luévano-Hipólito [a], A. Martínez-de la Cruz [a,*], Q.L. Yu [b], H.J.H. Brouwers [b]

[a] CIIDIT, Facultad de Ingeniería Mecánica y Eléctrica, Universidad Autónoma de Nuevo León, Ciudad Universitaria, C.P. 66451 San Nicolás de los Garza, N.L., Mexico
[b] Department of the Built Environment, Eindhoven University of Technology, PO Box 513, 5600 MB Eindhoven, The Netherlands

ABSTRACT

$Bi_2Mo_3O_{12}$ oxide was prepared by co-precipitation method at 250 °C. The successful formation of the oxide was determined by X-ray powder diffraction (XRD) and its physical properties were studied using scanning electron microscopy (SEM), diffuse reflectance spectroscopy (DRS) and adsorption–desorption N_2 isotherms (BET). $Bi_2Mo_3O_{12}$ sample was composed of agglomerates of primary particles with faces and edges well defined. The oxide exhibited excellent performance for the removal of nitric oxide (NO) from air, reaching a percentage remove of 88.9% in steady state under UVA light irradiation. The synergetic effect between $Bi_2Mo_3O_{12}$ and Bi_2MoO_6 phases was also investigated for this reaction. The results indicated that Bi_2MoO_6 is less active than $Bi_2Mo_3O_{12}$ for the photocatalytic removal of NO under same experimental conditions.

© 2013 Elsevier B.V. All rights reserved.

1. Introduction

Within Bi_2O_3–MoO_3 binary system, α-$Bi_2Mo_3O_{12}$, β-$Bi_2Mo_2O_9$, and γ-Bi_2MoO_6 phases have been recognized as efficient catalysts for the oxidation of propylene to acrolein [1] and for the conversion reaction of 1-butene to butadiene and 2-butene [2]. Bismuth molybdates have also found applications as ionic conductors [3], optics [4], acoustic-optical [5], photoconductors [6] and gas sensors [7]. In recent years, the photocatalytic activity of bismuth molybdates has been tested for several chemical reactions in aqueous media under UV and Visible light irradiation [8–10].

Among these bismuth molybdates, α-$Bi_2Mo_3O_{12}$ oxide has a deficient oxygen fluorite structure with Mo in MoO_4 tetrahedra and vacancies every three Bi sites [11,12]. These vacancies are in an ordered arrangement at room temperature within the infinite Bi channels and with three different Mo sites, each of which is coordinated by five O atoms. The Bi and Mo are concentrated in parallel layer to (1 0 1) plane that intersect the lattice parameter, *b* at approximately 1/8, 3/8, 5/8 and 7/8 (Fig. 1). Previous studies have shown that the lay of Bi and Mo sites in the same plane seems to be important for redox features of Mo and Bi sites, i.e. some electrons can transfer between them during reactions [14].

Previously, we have investigated the photocatalytic activity of $Bi_2Mo_3O_{12}$ oxide prepared by different methods for the

degradation of rhodamine B molecules in aqueous solution under visible light irradiation [11,15]. To the best of our knowledge no study has been reported on the photocatalytic removal of NO_x using $Bi_2Mo_3O_{12}$ as photocatalyst. However, the isostructural tungstate phase of Bi_2MoO_6, with chemical formula Bi_2WO_6 was reported for NO removal under visible and solar light irradiation [16]. In the current work, the photocatalytic activity of $Bi_2Mo_3O_{12}$ oxide was tested under UVA irradiation for NO removal from air under different experimental conditions. The synergistic effect between $Bi_2Mo_3O_{12}$ and Bi_2MoO_6 was also investigated.

2. Experimental

2.1. Synthesis of $Bi_2Mo_3O_{12}$

$Bi_2Mo_3O_{12}$ oxide was synthesized by co-precipitation method following a procedure previously reported [15]. The synthesis route implies the preparation of two aqueous solutions of inorganic salts. In the first one, 1.33×10^{-2} mole of $Bi(NO_3)_3 \cdot 5H_2O$ (Aldrich, 99%) were dissolved under continuous stirring in 100 mL of HNO_3 (10% v/v). In the second one, 2.86×10^{-3} mole of $(NH_4)_6Mo_7O_{24} \cdot 4H_2O$ (Aldrich, 99%) were dissolved under continuous stirring in 100 mL of 2 M NH_4OH solution. The $Bi(NO_3)_3 \cdot 5H_2O$ solution was added dropwise into $(NH_4)_6Mo_7O_{24} \cdot 4H_2O$ solution with vigorous stirring and the pH of the solution was adjusted to 9 by using NH_4OH. The resulting yellow suspension was maintained at 100 °C to promote the evaporation of the solvent. The yellow powder obtained was heated at 250 °C for 24 h to obtain the polycrystalline powders of

* Corresponding author. Tel.: +52 81 83 29 40 20; fax: +52 81 83 32 09 04.
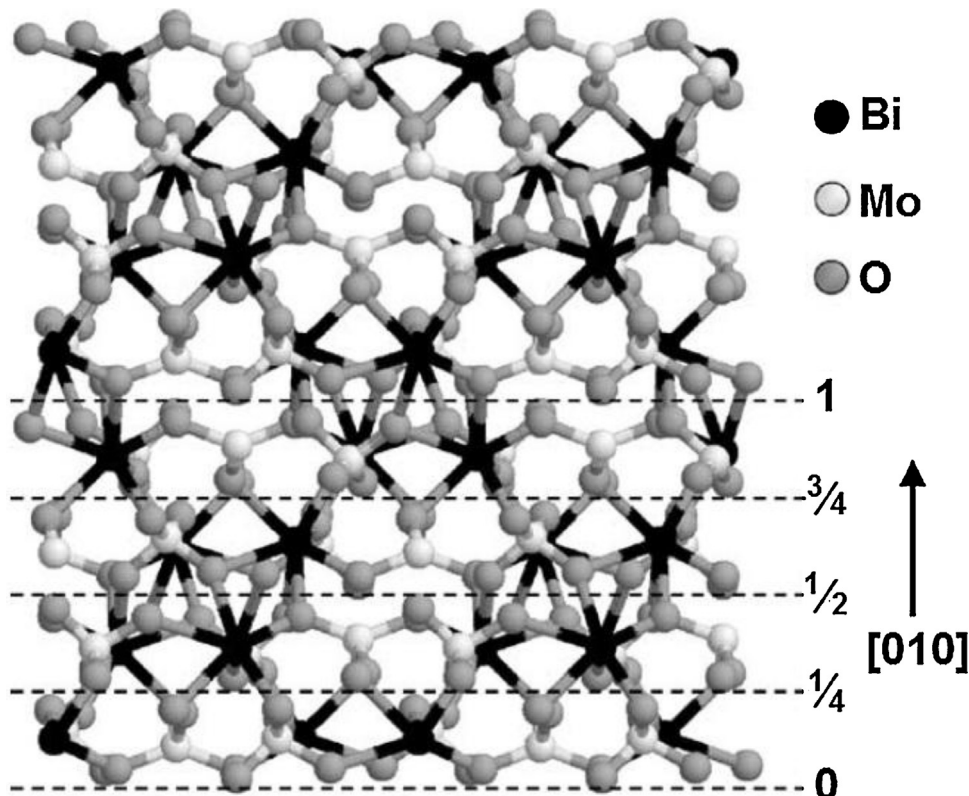*E-mail address:* azael70@yahoo.com.mx (A.M.-d.l. Cruz).

Fig. 1. Layers of $Bi_2Mo_3O_{12}$ viewed along $\langle 1\,0\,0 \rangle$ [13].

$Bi_2Mo_3O_{12}$. Then, the sample was washed with distilled water for several times and dried at $100\,°C$, which hereafter will be labeled as COP250. For comparative purposes, $Bi_2Mo_3O_{12}$ oxide was also synthesized by melting stoichiometric amounts of Bi_2O_3 (Aldrich, 99%) and MoO_3 (Aldrich, 99%) at $700\,°C$ for 24 h (MELT700) [17]. After cooling the formed crystals were ground into powder. In the same way, Bi_2MoO_6 was prepared by co-precipitation method at $450\,°C$ following a procedure described in a previous work [8]. It should be noted that for the synthesis of $Bi_2Mo_3O_{12}$ and Bi_2MoO_6 by co-precipitation method, the lowest temperature was chosen in which the oxides were obtained in pure form.

2.2. Characterization

The structural characterization of $Bi_2Mo_3O_{12}$ oxide was carried out by X-ray powder diffraction using a Bruker D8 Advance diffractometer with a Cu K_α radiation (40 kV, 30 mA), a typical run was made with a $0.05°$ step size and a dwell time of 0.5 s. The morphology of the synthesized oxide was analyzed by scanning electron microscopy using a FEI Nova NanoSEM 200 with an accelerating voltage of 30 kV. The UV–Vis diffuse reflectance absorption spectra of the samples were obtained using a UV–Vis spectrophotometer Perkin–Elmer Lambda 35 equipped with an integrating sphere. The BET surface area measurements were carried out by adsorption–desorption N_2 isotherms by means of a Bel-Japan Minisorp II surface area and pore size analyzer. The isotherms were evaluated at $-196\,°C$ after a pretreatment of the samples at $150\,°C$ for 24 h.

2.3. Photocatalytic experiments

The photocatalytic oxidation of nitric oxide was carried out in a laboratory test set-up designed according to standard ISO 22197-1:2007 (Fig. 2). The experimental setup consisted of a planar reactor cell ($20 \times 10 \times 3$ cm), an UVA light source, a chemiluminescent NO_x analyzer, and a gas supply. The samples for photocatalytic oxidation tests were prepared by coating an aqueous suspension of the oxide on glass substrate with an area of 20×10 cm. The photocatalyst was applied on the glass substrate by brush coating using colloidal silica as binder. The weight ratio in the suspension was 0.1:0.1:0.8 for the photocatalyst, colloidal silica and water, respectively. The coated substrate was then exposed at $100\,°C$ in a ventilated oven to remove water from suspension. The mass of the photocatalyst used for each experiment was fixed at 0.4 g. NO gas was used as target pollutant, and consisted of 50 ppm NO stabilized in N_2. The final NO concentration was diluted to 500 ppb using air which was composed of 20.5 vol% of O_2 and 79.5 vol% of N_2. The flow rate of gas throughout the reactor was $1\,L\,min^{-1}$ and the residence time was 3.6 s. The temperature and relative humidity of the reactor were controlled at $20 \pm 1\,°C$ and 50%, respectively. Two additional experiments were done modifying the relative humidity at 30 and 70% to study its effect in NO photooxidation process. Three lamps of UVA (Philips) were used as light source with an irradiance of $10\,W\,m^{-2}$. The NO_x concentration was analyzed using a chemiluminescent NO_x analyzer (HORIBA 370) with a sampling rate of $0.8\,L\,min^{-1}$. A more detailed information about the test set-up and experimental procedure can be found elsewhere [18–20].

3. Results and discussion

3.1. Characterization

The XRD patterns of $Bi_2Mo_3O_{12}$ oxide prepared by melting oxides (MELT700) and co-precipitation method (COP250) are shown in Fig. 3. All diffraction lines in both XRD patterns can be indexed on the basis of $Bi_2Mo_3O_{12}$ structure according to the JCPDS card No. 21-0103. Additional diffraction lines due to the impurities were not detected.
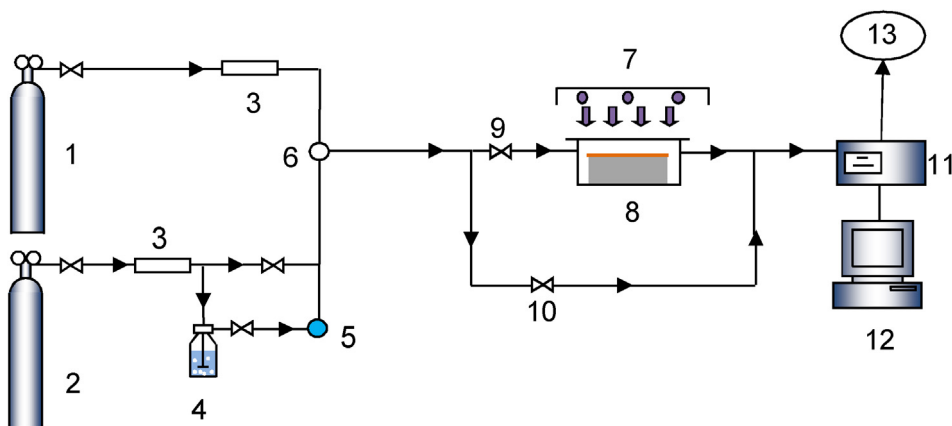
Fig. 2. Schematic diagram of the photocatalytic degradation set-up. (1) NO gas supply; (2) synthetic air; (3) mass controller meter; (4) humidifier; (5) humidity controller; (6) temperature and relative humidity sensor; (7) light source; (8) reactor; (9) valve; (10) valve; (11) NO$_x$ analyzer; (12) computer; (13) vent.
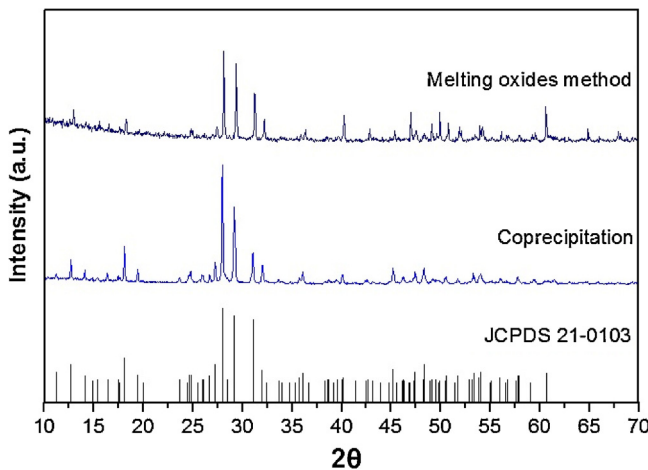

Fig. 3. XRD patterns of the Bi$_2$Mo$_3$O$_{12}$ samples prepared by co-precipitation at 250 °C and by melting oxides at 700 °C.

Table 1
Properties and kinetic data of Bi$_2$Mo$_3$O$_{12}$ samples prepared by different methods.

Sample		E_g (eV)	BET surface area	
			(m^2 g^{-1})	k' (min^{-1})
Bi$_2$Mo$_3$O$_{12}$	Melting oxides (MELT700)	2.73	0.2	0.07
	Co-precipitation (COP250)	2.70	8.8	0.63
Bi$_2$MoO$_6$	Co-precipitation (COP450 °C) [17]	2.44	2.3	0.10

The BET analysis revealed a specific surface area of 8.8 m^2 g^{-1} for COP250 and 0.2 m^2 g^{-1} for MELT700. The smaller surface area obtained by melting oxides method can be associated with the high temperature of reaction used that promotes a sintering process. According to the classification of adsorption isotherms, the profile of the adsorption–desorption curves for both samples corresponding with the type II isotherm, indicating a non porous material with a high energy of adsorption [21]. Diffuse reflectance of samples was analyzed by UV–vis spectroscopy. The band gap energy, E_g, obtained were 2.73 and 2.70 eV for MELT700 and COP250 , respectively (see Table 1). These values are within a typical range of 2.45–2.82 eV reported by Bi$_2$Mo$_3$O$_{12}$ prepared by different methods at different temperatures [15].

3.2. Photocatalytic activity

Photocatalytic activity of Bi$_2$Mo$_3$O$_{12}$ oxide supported on glass was investigated for NO removal at ambient conditions, i.e. $T = 20 \pm 1$ °C, $RH = 50 \pm 1\%$, and an inlet NO concentration of 500 ppb. Fig. 5 shows NO conversion (%) at different irradiation times for the samples COP250 and MELT700. Under UVA light irradiation, NO

Some selected SEM images of Bi$_2$Mo$_3$O$_{12}$ samples are shown in Fig. 4. For comparative purposes, the morphology of MELT700 is shown in Fig. 4(a). In this sample, irregular agglomerates were observed with about 100 μm in size due to that it was obtained from a melting medium. The sample COP250, see Fig. 4(b), is formed of agglomerates of primary particles with faces and edges well defined. Also, it can be seen that the presence of holes formed possibly due to the evolution of NH$_3$, O$_2$ and H$_2$O gases during the thermal treatment (Fig. 4(c)).
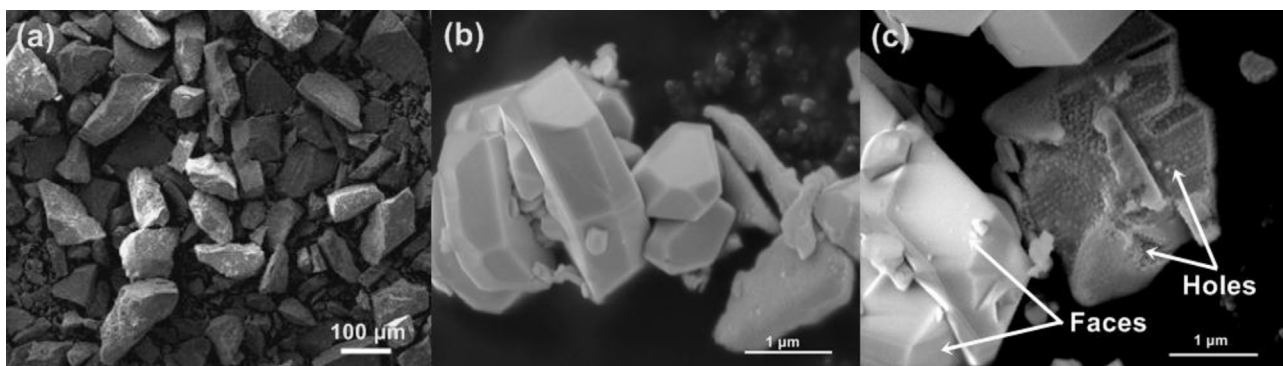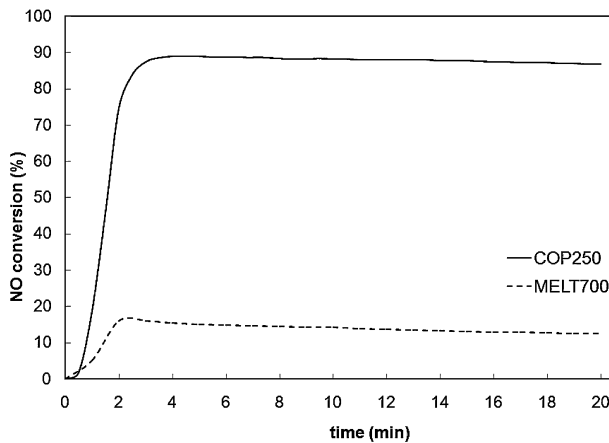

Fig. 4. SEM images of the Bi$_2$Mo$_3$O$_{12}$ samples prepared by (a) melting oxides at 700 °C and (b) and (c) co-precipitation at 250 °C.

Fig. 5. NO conversion (%) using $Bi_2Mo_3O_{12}$ oxide prepared by different methods as photocatalyst. (UVA, $\tau_R = 3.6$ s, $Q = 1$ L min^{-1}, $E = 10$ W m^{-2}).

removal quickly reached a steady state of 88.9% within 4 min in the presence of $Bi_2Mo_3O_{12}$ (COP250), whereas NO removal using the sample MELT700 only reached 16%. The above results reveal a much higher photocatalytic activity of the sample prepared by co-precipitation method due to its preparation method at low temperature which leads to a material with higher surface area, and low particle size compared to the reference method. The results are summarized in Table 1.

In Fig. 6, the changes in NO, NO_2 and NO_x concentration during their photocatalytic conversion using COP250 as photocatalyst are shown. After the adsorption–desorption equilibrium of the gases on the photocatalyst surface was reached, the lamp was turned on, and the NO concentration dropped rapidly and reached a steady state in 4 min. According with the results, an increase in the NO_2 concentration was observed which could be explained by the oxidation of NO to NO_2 on the photocatalyst surface. The total NO_x concentration, which is the sum of NO and NO_2 concentrations was also decreased. The NO_2 generated was 37% of the NO removed and the remained (63%) possibly was oxidized into nitrite and nitrate ions (NO_2^-/NO_3^-) and were fixed on the surface of the photocatalyst as was reported in previous papers [22–24].

Additional experiments were done in order to investigate the effect of relative humidity on the photocatalytic oxidation efficiency, and the results are shown in Fig. 7. When the relative humidity was increased from 30% to 50%, NO removal (%) was
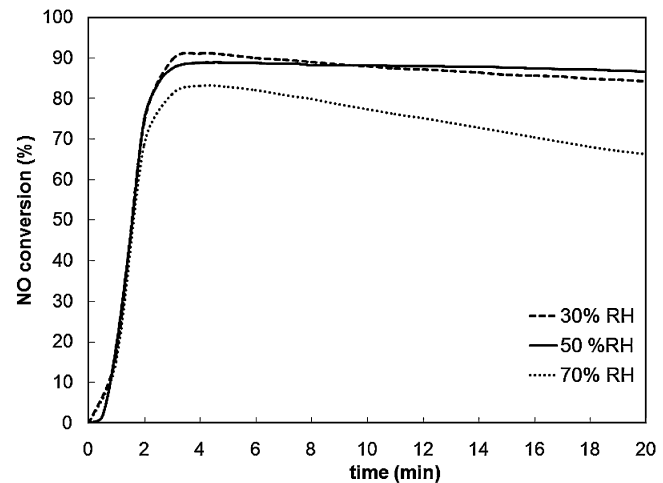

Fig. 7. NO conversion (%) using $Bi_2Mo_3O_{12}$ as photocatalyst with different relative humidities. (UVA, $_R = 3.6$ s, $Q = 1$ L min^{-1}, $E = 10$ W m^{-2}).

almost the same. However, at high relative humidity (70%) NO removal (%) decreased rapidly possibly due to the competition for adsorption sites of the $Bi_2Mo_3O_{12}$ surface between nitric oxide and water.

In literature, there are some studies about the synergistic effect of the $Bi_2Mo_3O_{12}$ and Bi_2MoO_6 as catalysts in the oxidative dehydrogenation of C_4 raffinate-3 [25] and the partial oxidation of propylene to acrolein [26]. In the later work, the authors proposed a remote control mechanism, in which oxygen species formed on the Bi_2MoO_6 surface migrate onto the surface of $Bi_2Mo_3O_{12}$ to create active sites. In an attempt to investigate the synergistic effect of these photocatalysts on NO removal capacity, a mixture consisting of $Bi_2Mo_3O_{12}$ and Bi_2MoO_6 was prepared by a mechanical mixing method (50/50 wt%), and applied as photocatalyst for the NO removal under UVA light irradiation. The mechanical mixture was simply ground to prepare the mixed photocatalyst. Unlike previous works in catalysis field, $Bi_2Mo_3O_{12}$ showed higher photocatalytic activity than Bi_2MoO_6 and the synergetic catalytic effect was not observed, as can be seen in Fig. 8. This result can be associated with the difference in the number of absorbed photons because of the larger surface area of $Bi_2Mo_3O_{12}$. This can contribute to make $Bi_2Mo_3O_{12}$ more able to absorb NO molecules to react with hydroxyl radicals generated in the photocatalytic process and thus transform the nitric oxide to nitric dioxide and then to nitric acid to form nitrate ion [27]. According to the literature, bismuth
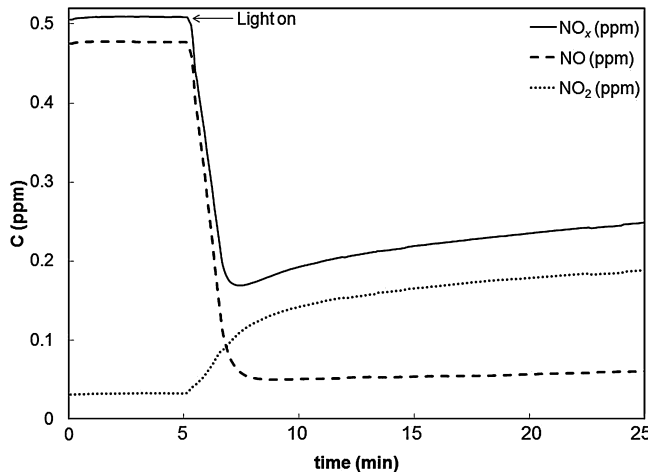

Fig. 6. Evolution of the NO, NO_2 and NO_x concentration during the course of their photocatalytic conversion. (UVA, $\tau_R = 3.6$ s, $Q = 1$ L min^{-1}, $E = 10$ W m^{-2}).

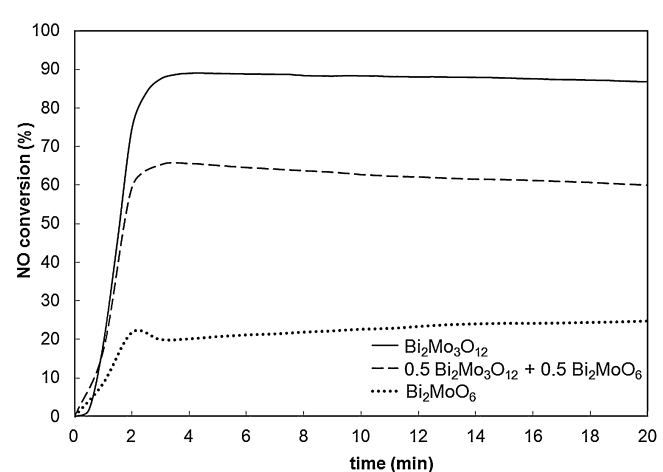**Fig. 8.** NO conversion (%) of $Bi_2Mo_3O_{12}$, Bi_2MoO_6, and its mixture as a function of time. (UVA, $\tau_R = 3.6$ s, $Q = 1$ L min^{-1}, $E = 10$ W m^{-2}).

molybdates are not active for H_2 generation from an aqueous methanol solution possibly due to their conduction bands levels are not more negative than the potential needed for water reduction to form H_2 [28]. However, bismuth molybdates are active for O_2 generation from an aqueous silver nitrate solution. Therefore, the oxidation of NO using $Bi_2Mo_3O_{12}$ as photocatalyst can be explained by a mechanism that involves direct reaction between the photogenerated electrons and oxygen molecules to form superoxide ion and consequently to form hydroxyl radicals.

On the basis of these results, $Bi_2Mo_3O_{12}$ oxide prepared by a simple co-precipitation method at low temperature can be considered as efficient photocatalyst to remove nitric oxide from air.

4. Conclusions

$Bi_2Mo_3O_{12}$ oxide was prepared by co-precipitation method at low temperature (250 °C) and at high temperature (700 °C) by melting oxides method. The resulting oxides consisted of particles with different morphologies and physical properties such as surface area and particle size. The oxides prepared by these methods were used as photocatalysts in the photocatalytic removal of NO from air at ambient conditions. The oxide prepared by co-precipitation showed higher efficiency in NO removal than the oxide prepared by the melting oxides method reaching 88.9% of NO conversion in steady state under UVA light irradiation. The efficiency of the photocatalytic reaction was adversely affected as the relative humidity went higher than 50% due to the competition in the adsorption sites on the $Bi_2Mo_3O_{12}$ surface between nitric oxide and water molecules. The synergistic effect of $Bi_2Mo_3O_{12}$ and Bi_2MoO_6 was also investigated in this reaction. The results showed that the synergistic effect was not observed and the $Bi_2Mo_3O_{12}$ exhibited higher photocatalytic efficiency than the Bi_2MoO_6 due to its higher surface area and its abundant adsorption sites for NO adsorption.

Acknowledgments

References

[1] D. He, W. Ueda, Y. Moro-Oka, Catal. Lett. 12 (1992) 35–44.
[2] A. Bhakoo, G.C. Bond, R.D. Rees, B. Sauerhammer, A.O. Taylor, I. York, Catal. Lett. 57 (1999) 55–60.
[3] R.N. Vannier, F. Abraham, G. Nowogrocki, G. Mairesse, J. Solid State Chem. 142 (1999) 294–304.
[4] V. Marinova, M. Veleva, Opt. Mater. 19 (2002) 329–333.
[5] D.K. Biegelsen, T. Chen, J.C. Zesch, J. Appl. Phys. 46 (1975) 941–942.
[6] T. Sekiya, A. Tsuzuki, Y. Torti, Mater. Res. Bull. 21 (1985) 601–608.
[7] N. Hykaway, W.M. Sears, R.F. Frindt, S.R. Morrison, Sens. Actuators, B 15 (1988) 105–118.
[8] A. Martínez-de la Cruz, S. Obregón, J. Mol. Catal. A: Chem. 320 (2010) 85–91.
[9] H. Li, K. Li, H. Wang, Mater. Chem. Phys. 116 (2009) 134–142.
[10] L. Zhang, T. Xu, X. Zhao, Y. Zhu, Appl. Catal., B 98 (2010) 138–146.
[11] A. Martínez-de la Cruz, S.M.G.M. Villarreal, L.M. Torres-Martínez, E.L. Cuéllar, U.O. Méndez, Mater. Chem. Phys. 112 (2008) 679–685.
[12] A.F.D. van den Elzen, G.D. Rieck, Acta Crystallogr., Sect. B: Struct. Sci. 29 (1973) 2433–2436.
[13] S.V. Yanina, R.L. Smith, J. Catal. 213 (2003) 151–162.
[14] T. Ono, K. Utsumi, M. Kataoka, Y. Tanaka, F. Noguchi, Catal. Today 91 (2004) 181–184.
[15] A. Martínez-de la Cruz, S. Obregón, Solid State Sci. 11 (2009) 829–835.
[16] Y. Huang, Z. Ai, W. Ho, M. Chen, S. Lee, J. Phys. Chem. C 114 (2010) 6342–6349.
[17] M. Malys, G. Fafilek, C. Pirovano, R.N. Vannier, Solid State Ionics 176 (2005) 1733–1769.
[18] Q.L. Yu, H.J.H. Brouwers, Appl. Catal., B 92 (2009) 454–461.
[19] G. Hüsken, M. Hunger, H.J.H. Brouwers, Build. Environ. 44 (2009) 2463–2474.
[20] M.M. Ballari, M. Hunger, G. Hüsken, H.J.H. Brouwers, Appl. Catal., B 95 (2010) 245–254.
[21] J.B. Condon, Surface Area and Porosity Determinations by Physisorption, Elsevier, Amsterdam, 2006, pp. 11–13.
[22] J.C. Jung, H. Lee, H. Kim, Y. Chung, T.J. Kim, S.J. Lee, S. Oh, Y.S. Kim, I.K. Song, J. Mol. Catal. A: Chem. 271 (2007) 261–265.
[23] T. Ibusuki, K. Takeuchi, J. Mol. Catal. A: Chem. 88 (1994) 93–102.
[24] T. Martinez, A. Bertron, E. Ringot, G. Escadeillas, Build. Environ. 46 (2011) 1808–1816.
[25] T. Sano, N. Negishi, K. Koike, K. Takeuchi, S. Matsuzawa, J. Mater. Chem. 14 (2004) 380–384.
[26] Z. Bing, S. Pei, S. Shishan, G. Xiexian, J. Chem. Soc., Faraday Trans. 86 (1990) 3145–3150.
[27] M.M. Ballari, Q.L. Yu, H.J.H. Brouwers, Catal. Today 161 (2011) 175–180.
[28] Y. Shimodaira, H. Kato, H. Kobayashi, A. Kudo, J. Phys. Chem. B 110 (2006) 17790–17797.